PROCEEDINGS, 44th Workshop on Geothermal Reservoir Engineering
Stanford University, Stanford, California, February 11-13, 2019
SGP-TR-214

Experimental Evaluation of Effect of Hydro-Shearing on Fracture Conductivity at The Utah FORGE Site

Nadimi[1], S., Forbes[2], B., Moore[2], J., Ye[3], Z., Ghassemi[3], A. and McLennan[4], J. D.

[1] Seismos Inc., Palo Alto, CA

[2]EGI, University of Utah, Salt Lake City, UT

[3]Department of Petroleum Engineering, University of Oklahoma, Norman, OK

[4]Department of Chemical Engineering, University of Utah, Salt Lake City, UT

[1]nadimisiavash@gmail.com

Keywords: hydro-shearing, artificial shearing, stress-dependent, FORGE Utah, conductivity, well 58-32, and EGS

ABSTRACT

Laboratory fracture conductivity tests were performed to investigate the effects of temperature, time and lateral offset (sliding) on the conductivity of a representative fracture under in situ conditions experienced at the DOE's FORGE (Frontier Observatory for Research in Geothermal Energy) site, near Milford, Utah. Conductivities of artificially sheared (shifted) fractures were compared to conductivities before shear displacement and the resultant dilation. Three types of injection tests were performed: 1) stress-dependent fluid flow tests under hydrostatic compression; 2) hydro-shearing tests under triaxial stress conditions and 3) fluid flow/conductivity testing at elevated temperature under hydrostatic confining pressure conditions. These experiments were performed on granitic core recovered from the thermal reservoir in well 58-32 at the Utah FORGE location.

The experimental results showed a significant increase in fracture conductivity after substantial shear displacement. The initial fracture conductivities were approximately two orders of magnitude larger in the sheared samples. Variation in conductivity depends on the mechanical and physical properties of the matrix and the fractures, including fracture roughness, and the size distribution of the associated asperities.

While conductivity was initially substantially larger, these laboratory experiments also showed a significant decrease in fracture conductivity over even relatively modest testing times. In one test, at ambient temperature, conductivity dropped to less than 20% of its measured initial value after only 100 hours of representative effective normal stress application. In all cases, the increase of normal stress on the fracture surface, and possibly thermal stresses along with the mechanical loading, led to fracture conductivity reduction. There is a direct correlation between measured roughness, conductivity magnitude immediately after shear displacement, and reduction in conductivity with time at load. Reservoir simulations should carefully consider this thermo-mechanical conductivity degradation. Future studies would be useful to evaluate injecting of a substantially cooler fluid and the influence of cyclic injection.

1. INTRODUCTION

Substantial research has been conducted to study fracture conductivity and rock permeability at elevated temperature, including laboratory testing. It is expected that native formation permeability decreases with increasing temperature (Moore et al., 1994; Yasuhara et al., 2006). According to Moore et al. (1994), dissolution of asperities, and filling of fractures and pores are among the main chemomechanical reasons for reduction of permeability in high-temperature environments. Increasing in situ stress with depth also reduces permeability significantly (for example, Ingebritsen and Manning, 2010). Fredd et al. (2000) evaluated the effects of normal stress on conductive flow through propped and unpropped fractures by using a standard fracture conductivity measurement cell. They found that the conductivity can vary by at least two orders of magnitude, depending on the rock properties, fracture roughness, size distribution of asperities, mechanical properties of the fracture, and mineralogy of the fracture surfaces.

Laboratory fracture conductivity and sheared fracture conductivity tests were conducted to investigate the effects of temperature, time, and sliding along natural fractures on the conductivity of a single fracture under reservoir conditions similar to those existing at the FORGE site. Conductivities of artificially sheared fractures were compared to conductivities of unsheared fractures under the same testing conditions. Three types of experimental tests were performed: 1) stress-dependent fluid flow/conductivity tests under hydrostatic compression; 2) hydro-shearing tests at room temperature in a triaxial apparatus, and 3) fluid flow testing on artificially sheared fractures at elevated temperature under hydrostatic confining pressure conditions. The setup for each experiment and the experimental results are discussed below.

2. FORGE

The Utah FORGE (Frontier Observatory for Research in Geothermal Energy) site has been chosen by the Department of Energy (DOE) as a field location for testing and demonstrating new technologies that advance geothermal heat extraction from low permeability host rocks. The FORGE site is located 350 km south of Salt Lake City and 16 km north-northeast of Milford, Utah, between the Basin and Range Province (BR) and the Colorado Plateau (CP). It is located 5 km west of the Roosevelt Hot Springs geothermal system, on gently

sloping alluvial fan deposits. The basement consists of a Tertiary granitic pluton exposed in the adjacent Mineral Mountains (Hardwick et al., 2016; Simmons et al., 2018). Well 58-32 was drilled and tested in 2017 to 7536 ft. The well encountered a static temperature of 199oC at total depth (Allis et al., 2019, Nadimi et al. 2018).

The main purpose of drilling well 58-32 was to measure the properties of the granitic reservoir at a depth where temperatures exceeded 175oC. In addition to temperature, rock type, permeability, fracture distributions and the orientations and magnitudes of the principal stresses were determined. In 2019, a series of injection tests will be conducted and monitored to supplement stimulation experiments conducted in 2017. Two new sub-horizontal wells will be drilled and hydraulically interconnected in the following years. Temperature measurements from existing wells, gravity surveys, a modern 3D seismic reflection survey, outcrop mapping, LiDAR analysis, seismic monitoring, analysis of core samples from well 58-32, and the testing and logging of the well have provided a comprehensive understanding of the geologic setting of the FORGE site. The core samples were used to infer reservoir properties and for experimental assessment of hydraulic shearing (Moore et al. 2018).

3. STRESS-DEPENDENT FLUID FLOW UNDER HYDROSTATIC COMPRESSION

Exploratory stress-dependent, fluid flow tests were carried out using a triaxial loading frame. This equipment has a maximum 300,000 lbf axial load capacity and a 20,000 psi confining pressure capacity. Control and data acquisition are automated. During the tests axial and lateral displacements were measured by strain-gauged cantilevers. Two orthogonal pairs of lateral cantilevers were used to measure the radial displacement; radial strain measurements were made perpendicular and aligned with the shearing fracture's trend. The pore pressure system of the equipment was used to apply injection pressure.

3.1. Sample Preparation and Setup

A unique sample geometry was prepared to enable hydraulic shearing. Figure 1 is a schematic of the testing setup. The purpose of testing reported here was to study shear stimulation of fractures in response to water injection (Nemoto et al., 2008; Bauer et al., 2016; Ye et al. 2017; Ye and Ghassemi 2018). The sample was a granite with a 30° precut and ground surface. Two screens in between the endcaps and the sample provided fluid access across the entire sample. The precut rock cylinder was drilled with 0.125-in diameter holes to opposing sides of the saw cut. The sample assembly is put inside the jacket and heat treated. The general testing protocols were as follows:

1- Cut a 1.5-inch diameter plug sample to a nominal 3-inch length.
2- Grind both ends to be flat and parallel to a tolerance of 0.0005 in.
3- Drill two 0.125-in diameter holes axially, one from each end, intersecting the plane where a crosscutting fracture will be cut.
4- Precut the sample at a 30° angle from the vertical.
5- Quantify the fracture roughness using optical profilometry. This is done before and after the testing.
6- Wrap the sample assembly in a shrink-fit Teflon jacket.
7- Place the specimen assembly in the pressure vessel, which is filled with hydraulic oil. The pressure inside the vessel (confining pressure) was increased to a specified level and allowed to stabilize.
8- Apply different constant confining and axial stresses.
9- Inject water and flow through the sample.
10- Apply pressure in discrete steps. The maximum applied injection pressure was maintained at 250 psi less than the confining pressure.
11- Measure displacement, stresses, flow rate, and pore pressure at the inlet and outlet (upstream and downstream) to sample.

The first test was conducted with the sample subjected to hydrostatic pressure conditions. Production and injection flow rate and displacement were measured under different confining and injection pressures with zero differential stress. The applied confining and injection pressures and the measured flow rate are shown in Figure 2. Strain under different confining pressures is presented in Figure 3.

3.2. Experimental Results

With an increase in the confining pressure from 2000 psi to 3000 psi, the flow rate decreased significantly as the fracture aperture was reduced by increasing normal stress. Even after subsequently reducing the confining pressure to 2500 psi and then to1500 psi, the flow rate did not recover (Figure 4). This may be due to rearrangement of the fracture asperity contacts and decreased fracture roughness. In order to magnify the behavior of the flow under higher confining pressures, the test result for 2000 psi confining pressure was removed from Figure 4 and presented in Figure 5. As shown in Figure 5, there is a linear relationship between the flow rate and the injection pressure at each confining pressure.

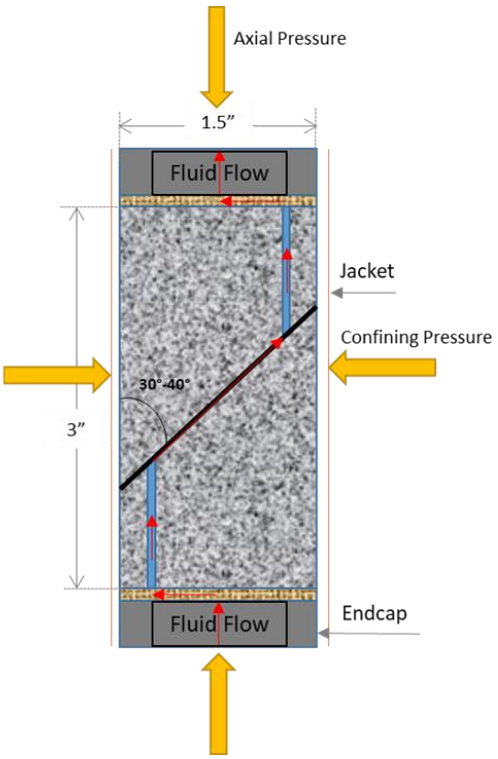

Figure 1. Schematic of the sample setup for stress-dependent fluid flow test and hydro-shearing test

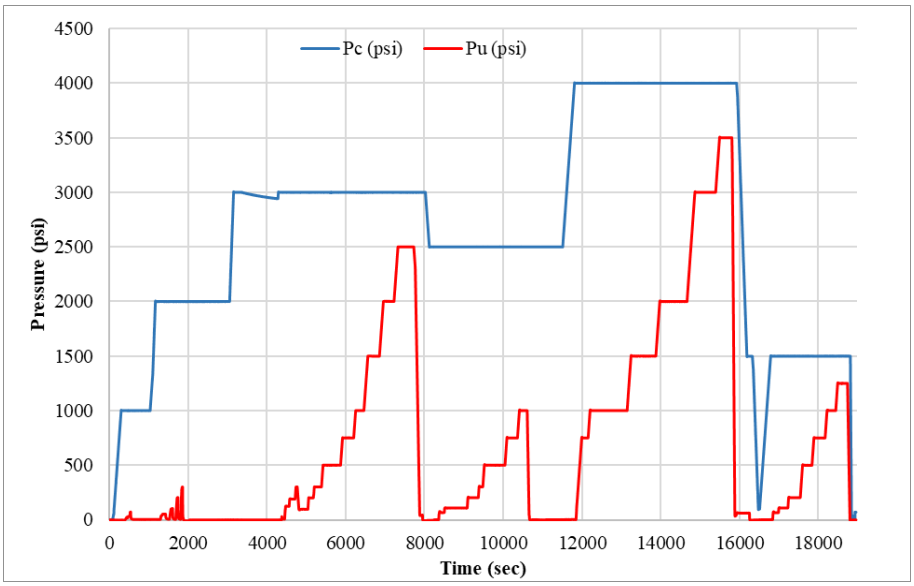

Figure 2. Test chronology and injection pressures for the saw cut sample in a hydraulic shearing test. The test was conducted under five different confining pressures (Pc= confining pressure, Pu=pore pressure or water pressure inside the fracture).

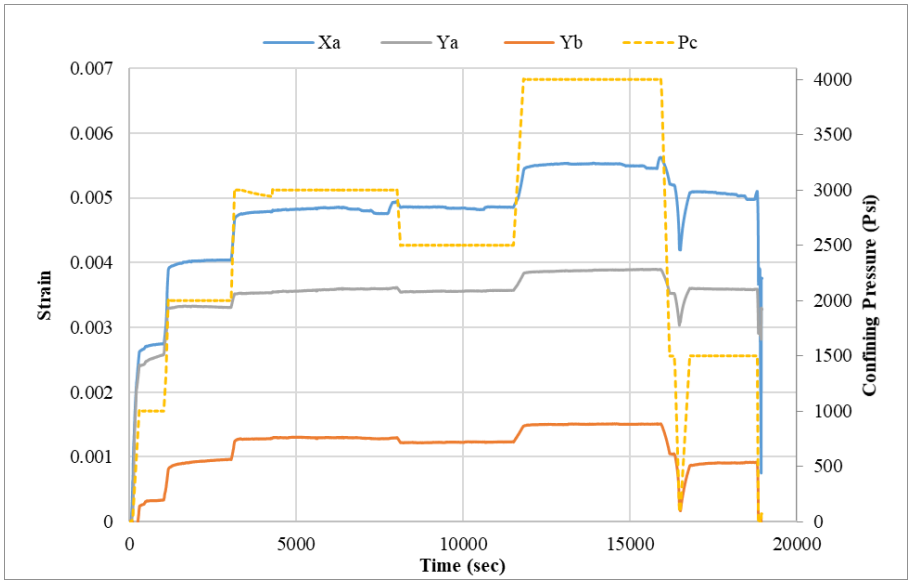

Figure 3. Strain for the saw cut sample in a triaxial hydro-shearing test under different confining pressures (Xa: axial strain, Ya and Yb: lateral strain, Pc: confining pressure).

The relationship between flow rate and confining pressure, corresponding to different injection pressures, is shown in Figure 6. Significant reduction of flow rate with an increase of confining pressure is evident. An approximate polynomial relationship (between flow rate and confining pressure) can be obtained from regression. An approximate polynomial relationship (between flow rate and confining pressure) can be obtained from regression.

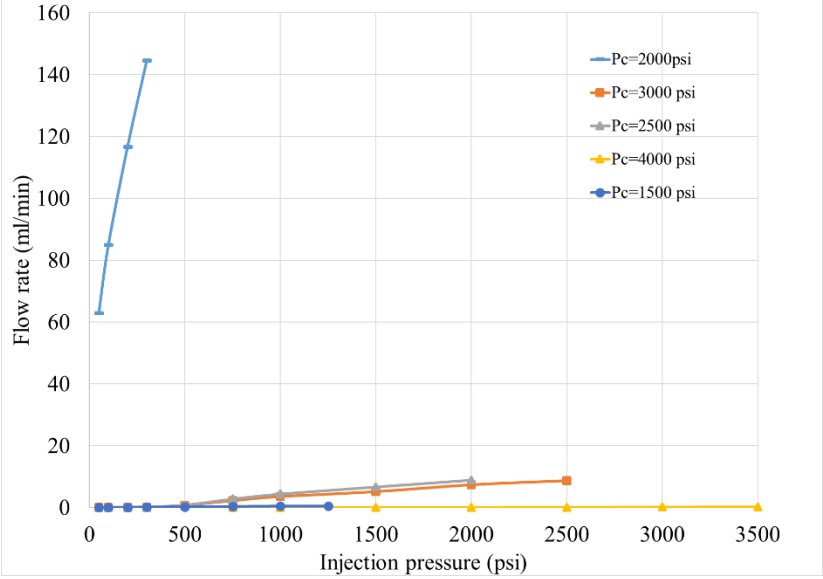

Figure 4. Flow rate (Q) versus injection pressure (P_{inj}) under different confining pressures for the saw cut sample.

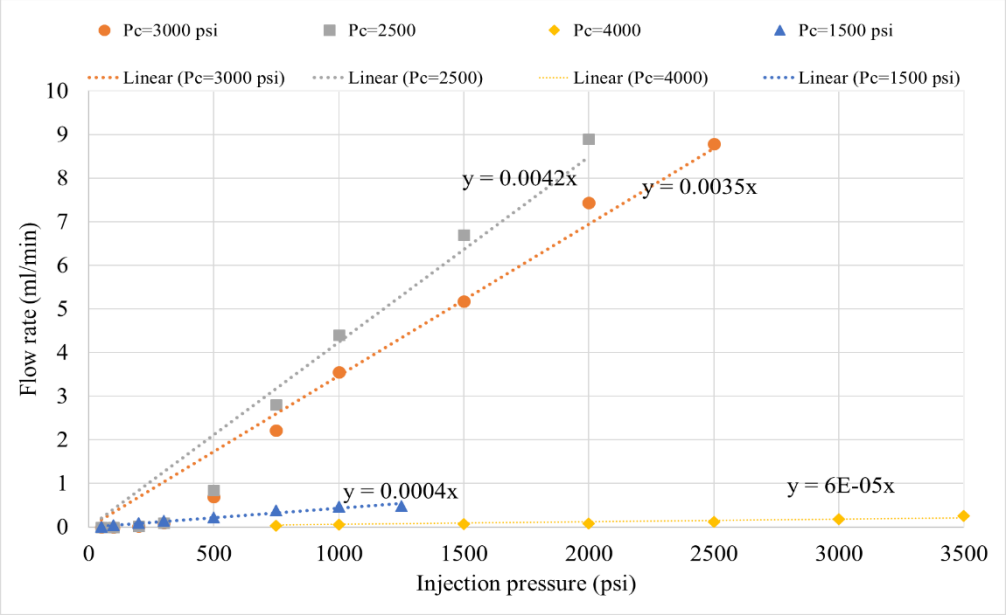

Figure 5. Flow rate versus injection pressure under different confining pressures for the saw-cut sample and linear fitted trend. With an increase in the confining pressure from 2000 psi to 3000 psi, the flow rate decreased significantly.

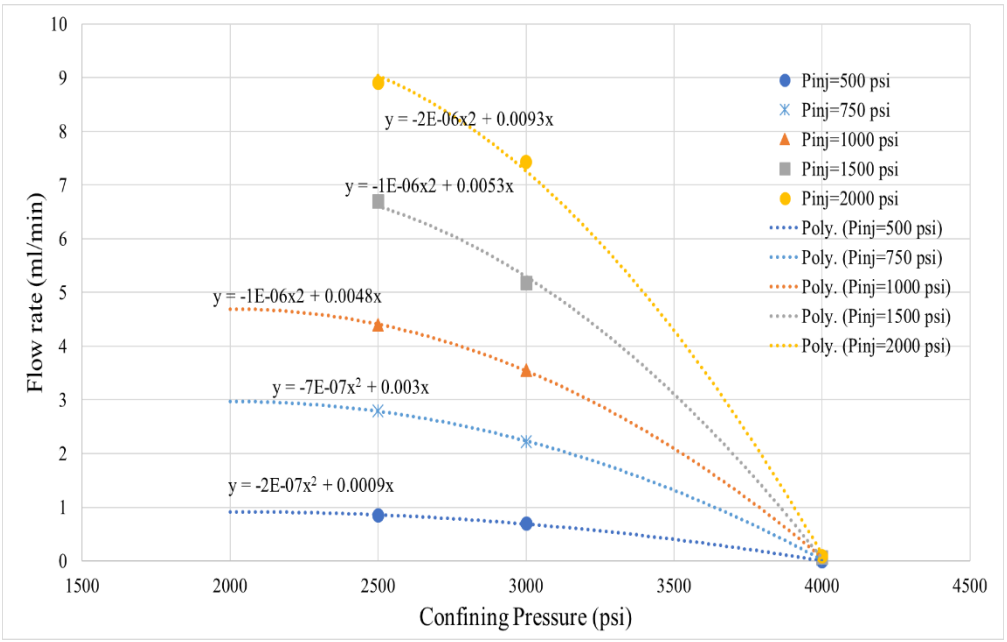

Figure 6. The relationship between flow rate and confining pressure, corresponding to different injection pressures for the saw-cut sample. The significant reduction of flow rate with an increase of confining pressure is evident.

4. HYDRO-SHEARING TEST UNDER TRIAXIAL STRESS CONDIDITONS

To evaluate the hydromechanical response of a fracture during injection-induced shear slippage, a hydro-shearing test was carried out on a saw-cut FORGE granite fracture. Figure 7 shows this fracture; with a Joint Roughness Coefficient (JRC) of 1.03. The experimental test setup is similar to the stress-dependent fluid flow test described earlier (see Figure 1). In this hydroshearing test, 4350 psi (30 MPa) confining pressure and 725 psi (5 MPa) initial injection pressure (provided by a syringe pump connected to the bottom borehole in the sample) were applied to the saw-cut fracture. The reason for this modest initial injection pressure is to completely saturate the fracture. Following this, the flow outlet was closed, preventing fluid from exiting the sample (see Figure 1). Next, the sample was loaded to a representative total in-situ stress state with 5500 psi (~38 MPa) differential stress. After that, as shown in Figure 1, the injection pressure was continuously increased from 725 psi (5 MPa) to 3625 psi (25 MPa) at a rate of 10 psi/s. This progressively reduced the effective normal stress. The purpose was to induce fracture slip during controlled stress relaxation. This stress relaxation is accompanied by measured microseismic events during fracture shearing (Ye et al., 2017, Ye & Ghassemi, 2018). Once the injection pressure reached 3625

psi (25 MPa), it was held constant for another ~220 seconds. More details related to the test system, the measurements and the experimental procedures can be found in Ye et al., 2017, and Ye & Ghassemi, 2018.

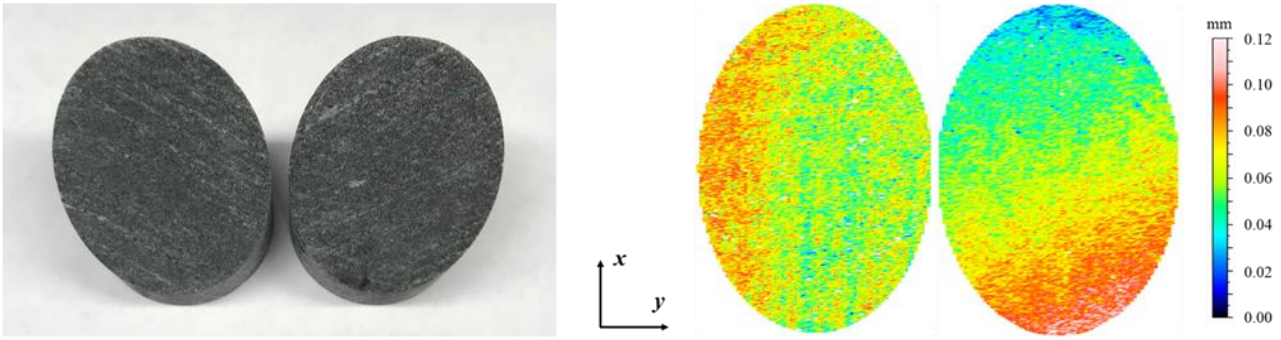

Figure 7. Saw-cut fracture and the laser scanning contour of the surfaces. The maximum surface relief is 0.12 mm, and the average JRC is 1.03).

The data from the saw-cut fracture are shown in Figure 8. The baseline deformation properties and fluid flow parameters in the pre-injection stage (initial application of confining pressure, axial loading, and injection pressure) are not shown. The displacements and flow rates were zeroed before injection. In Figure 8, the green curve represents the loading piston displacement of the test frame, which was kept constant under stress relaxation control. The blue curve is the injection pressure which was gradually increased from 725 psi to 3625 psi. The black curve describes the differential stress history which shows a significant drop once fracture slip is initiated. The red and pink curves are the normal dilation and shear slip of the fracture during the injection test. The effective normal stress and shear stress on the fracture plane are illustrated separately by the teal and dark-blue curves. The injection rate and the volume recorded on the injection pump are indicated by the purple curve and the brown curve, respectively. It is clear that the stresses, displacements, and flow rates vary with the changes in the injection pressure.

Based on changes in the injection pressure, evolution of the hydro-mechanical behavior in the test can be roughly divided into two stages: an injection pressure build-up stage (Stage 1) and an injection pressure hold stage (Stage 2). Characteristics of each stage are discussed below:

- Stage 1: The injection pressure was increased from 725 psi (5 MPa) to 3625 psi (25 MPa). This pressure ramping stage lasted from 0 s to ~280 s. Behavior during this stage can be separated into two parts. In the first part (from 0 s to ~190 s), the fracture was in a "*stick*" state. Changes in fracture normal dilation, shear slip and shear stress were negligible. A slight decrease of effective normal stress was caused by the increase in injection pressure. The injection rate was increased in a stable manner, and the flow rate curve did not fluctuate significantly. The pump volume decreased slightly. In the second part of this stage, the injection pressure was progressively increased to 3625 psi (25 MPa). Once the injection pressure exceeded 1740 psi (12 MPa), fracture slip initiated. In this "*slip*" state, rapid fracture shear slip and normal dilation occurred in conjunction with a significant stress drop. Consequently, the flow rate increased more rapidly, and more fluid entered the fracture due to the aperture increase that resulted from dilatant fracture slip. Since the injection pressure was prescribed to increase at a constant rate, the flow rate was automatically regulated by the pump to maintain constant pressure rate during injection. The fluctuations in flow rate (purple curve in Figure 8) during "slip" suggest permeability enhancement by fracture shearing. 0.09 mm of shear displacement and 0.01 mm of dilation normal to the fracture surface were accompanied by a 2750 psi (19 MPa) differential stress drop. Even though the saw-cut fracture had few asperities and its surface was relatively smooth, flow rate was still enhanced during the hydroshearing. Considering previous hydroshearing tests on rough-walled Sierra White granite fractures, the key to permeability enhancement by hydroshearing is asperity self-propping. Considering that the FORGE granite is relatively coarse grained and has nominally similar geomechanical properties to the Sierra White granite, enhancement of flow rate/permeability through hydroshearing would be expected.

- Stage 2: The injection pressure was held constant at 3625 psi (25 MPa) for another ~220 s. In this stage, fracture slip had terminated, and the changes in slip and dilation are second order. The displacements, differential stress, flow rate and pump volume remain constant since the injection pressure does not increase and the differential stress was released in stage 1. Therefore, the fracture was no longer in a critical stress condition and any slip was terminated.

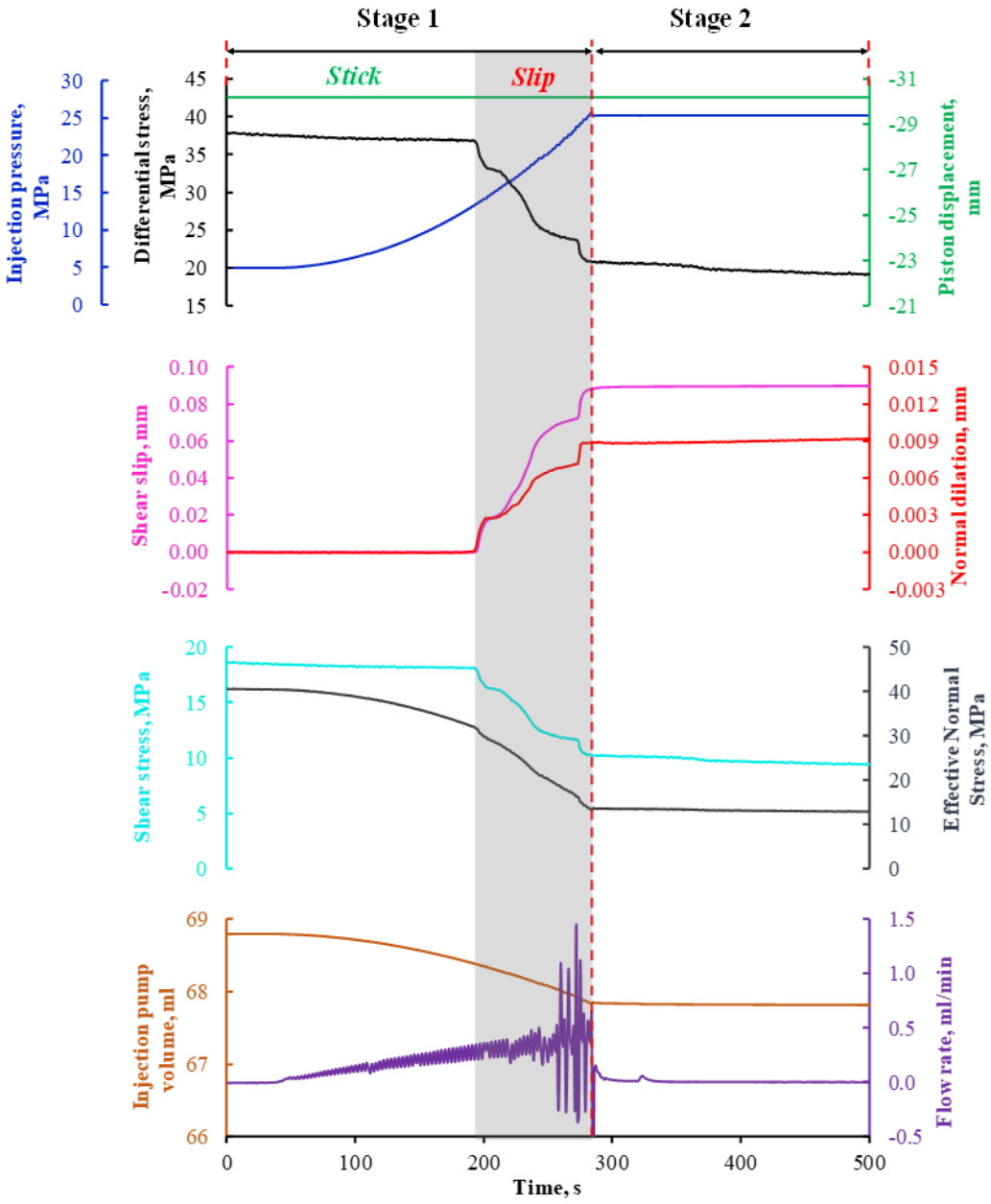

Figure 8. Hydro-mechanical measurements during a hydroshearing test on saw-cut fracture.

After the hydraulic shearing test, the saw-cut fracture was further subjected to a multistage triaxial shear test to determine the fracture's friction properties and the shear strength envelope. Since this artificial fracture was quite smooth, surface damage and frictional degradation resulting from the preceding hydroshearing test were neglected. The previous shear test was assumed to have no influence on the saw-cut fracture's friction coefficient and associated shear strength. During the multistage triaxial shear test, the flow inlet and outlet were connected to the atmosphere (see Figure 1). Confining pressure was progressive increased in stages and the axial differential stress was raised until the onset of fracture slip at each confining pressure stage. At each confining pressure stage, an axial differential stress is reached where fracture slip occurs. When slip occurs, the axial differential stress drops. After slip, the axial differential stress was removed and a new loading cycle was initiated at a higher confining pressure. Using the data from multiple confining pressure stages, a shear strength envelope was constructed. The stress-strain curve for the multistage test is shown in Figure 9(a), and the fracture failure envelope is shown in Figure 9(b). The friction coefficient is 0.42, for a friction angle of 23°. This low friction angle is consistent with a saw-cut fracture surface. Based on this multistage test, the normal stiffness (K_n) and shear stiffness (K_s) were also estimated at each confining pressure. These are compiled in Table 1. More information on this procedure can be found in Ye et al., 2016. The average normal and shear stiffnesses are 1.90×10^6 psi/in and 1.26×10^6 psi/in, respectively.

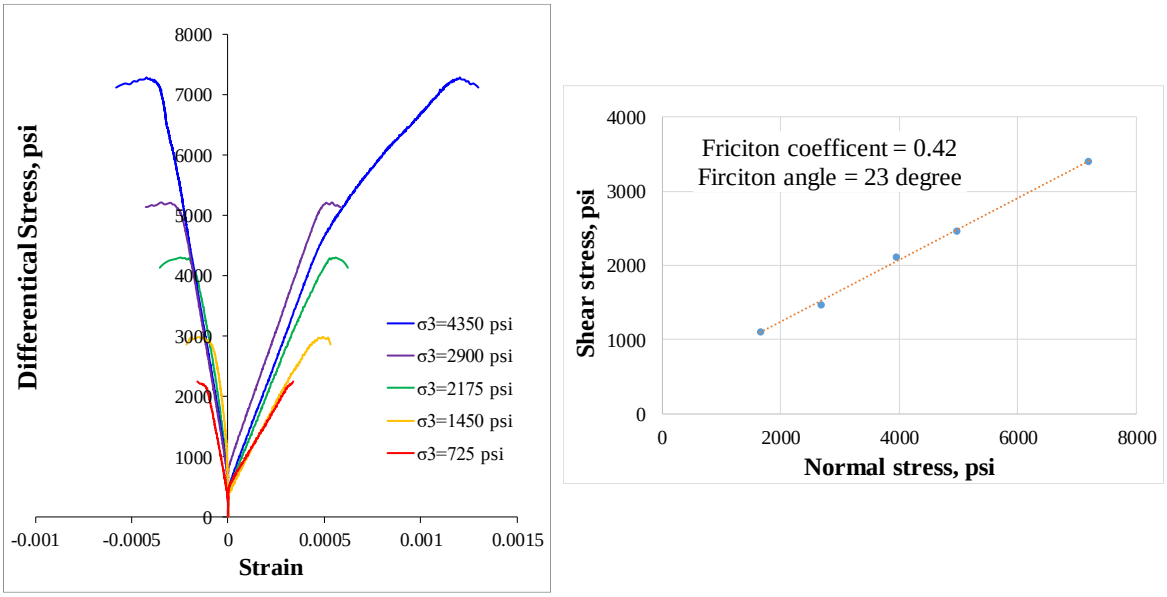

Figure 9. Results of a multistage triaxial shearing test on a saw-cut fracture, (a) stress-strain curve; (b) fracture failure envelope.

Table 1: Normal stiffness and shear stiffness of saw-cut Forge Fracture under multistage triaxial shear test.

Stiffness	Confining pressure, psi					Average value
	725	1450	2175	2900	4350	
K_n, $\times 10^6$ psi/in	1.55	1.44	2.11	2.17	2.20	1.90
K_s, $\times 10^6$ psi/in	1.05	1.08	1.35	1.38	1.45	1.26

5. FLUID FLOW THROUGH AN ARTIFICIALLY SHEARED FRACTURE AT ELEVATED TEMPERATURE

An experimental laboratory test was also carried out by applying simulated EGS reservoir conditions and conducting hydrostatic fracture conductivity tests on core samples. It provides a method for measuring fracture conductivity under elevated temperature, confining pressure, and pore fluid pressure (Stoddard et al., 2012).

5.1. Sample Preparation and Setup

Four 2.5-inch diameter granite samples from the Utah FORGE reservoir were prepared for this experimental study. A wedge was used to mechanically split the samples and create a rough fracture along each sample's axis (Figure 10). The samples were CT-scanned, and the roughness of the surfaces was calculated using MATLAB software. A CT-scanned profile is shown in Figure 11. The first measurement was performed on each sample with no axial shifting. That means that the opposing sides of the sample were precisely mated together and there was minimal asperity override. After measuring baseline conductivity under those conditions, to simulate potential shear displacement in a hydraulically sheared fracture, the opposing surfaces were axially shifted between 2 and 2.6 mm, and the opposite ends were ground so the pseudo-cylinder still had flat and parallel ends. This was intended to simulate a fracture subjected to shearing and propped only by asperities on the face of the fracture. The same hydraulic test conditions were applied to sheared and non-sheared samples to investigate the effect of hydro-shearing on fracture conductivity.

Based on the measured FORGE reservoir in-situ stresses, initial temperature estimates and pore pressure at a depth of 7400 ft, the static normal effective stress acting on the surface of a NE-SW striking fracture at the FORGE site is between approximately 1500 and 1800 psi, depending on the dip of the selected fracture. Various confining pressures in this range were applied to study the effects of effective normal stress on fracture conductivity. The initial testing was completed at ambient temperature. The temperature was then increased to 100°C and later to 175°C to correspond to temperatures at the depth ranges being tested. The samples remained at each temperature for at least 48 hours. The objective of these tests was to simulate possible downhole geothermal fluid flow behavior.

The experiments were conducted at flow rates of 5, 10, 15, 20, 25, and 30 ml/min. Each flow rate was maintained for at least for two minutes to ensure steady-state flow through the sample. The temperature of the injected water was 19°C. In order to ensure Darcy flow (laminar, linear, and single-phase flow), the flow rate was kept low. A summary of the tests under different confining pressure, flow rate, and temperature is presented in Table 2.

A general schematic of the experimental setup is shown in Figure 12. Two ISCO pumps were used for applying the confining and in-fracture, injection pressure. Hydrostatic confining pressure was applied with one pump. The second pump was used for flowing through the fracture. A back-pressure valve was installed on the outlet of the system to prevent the flowing fluid from vaporizing. A differential pressure transducer was installed in order to determine pressure drop. All of the connections in the system were plumbed with 1/8" NPT to 1/8" Swagelok fittings and 1/8" OD Swagelok tubing. LabView™ software along with a National Instruments NI CDAQ-9172 control board was used for data acquisition.

Figure 10. The two sides of a mechanically-split granite sample.

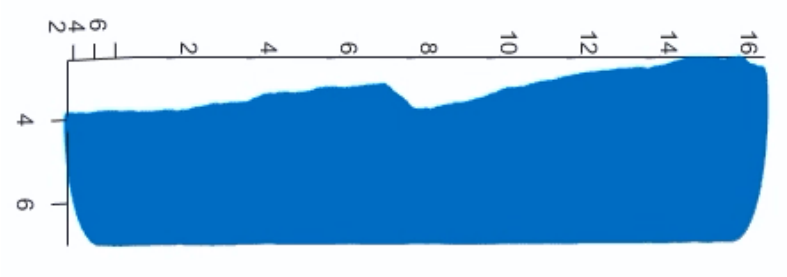

Figure 11. Side view of a CT-scanned surface. Each sample was CT-scanned to produce profiles of the fracture surfaces.

Table 2. Samples dimensions and basic test conditions for the elevated temperature hydraulic shearing experiments

Sample	**1**	**2**	**3**	**4**
Diameter (in)	2.5	2.5	2.5	2.5
Length (in)	6.25	6.31	7.03	6.9
Surface shift (in)	0.092	0.086	0.102	0.100
rms[1] (mm)	2.1254	2.8287	3.2437	3.6226
Temperature (°C)	Ambient, 100°C, 175°C, 100 °C, and Ambient[2]			
Confining pressure (psi)	1000, 1500, 2000, and 2500			
Flow rate mL/min)	5, 10, 15, 20, 25, and 30			

[1] Root mean square average of fracture surface roughness
[2] Cycle applied at each confining pressure

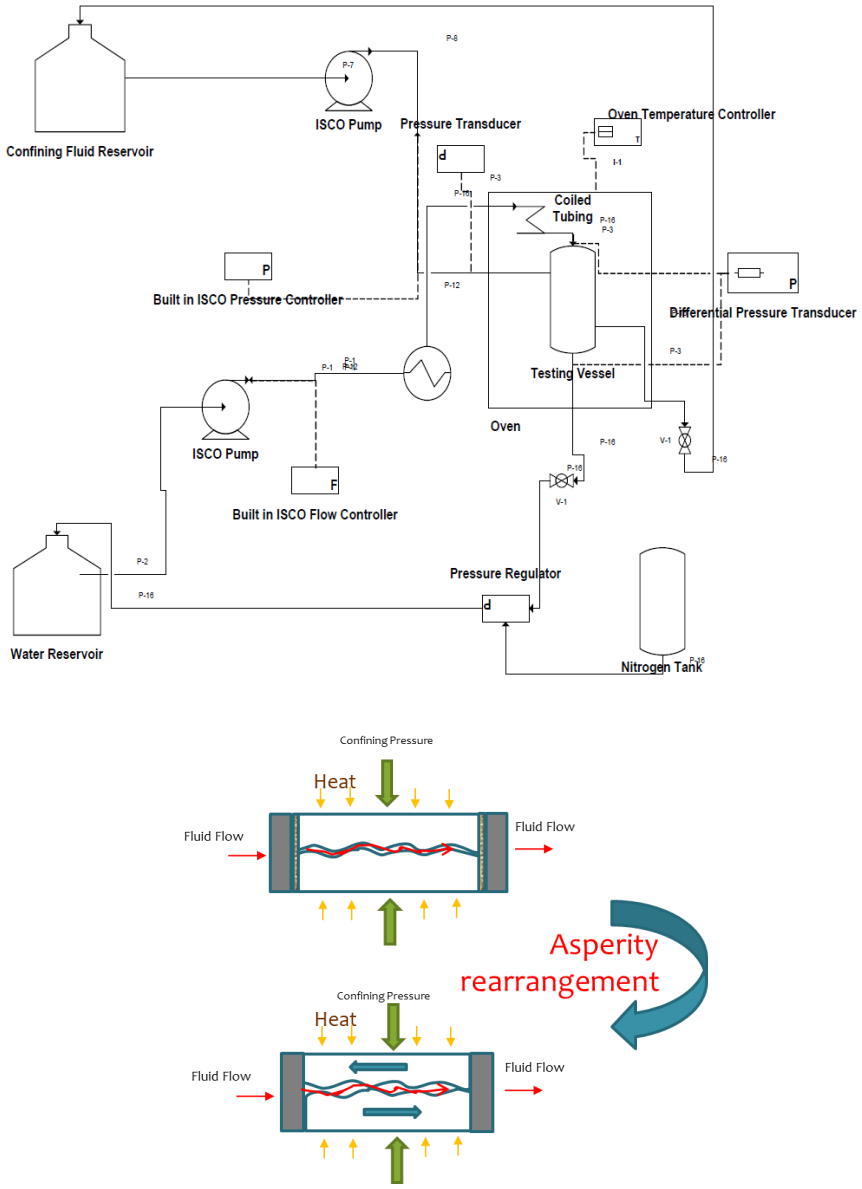

Figure 12. General schematic of the experimental setup for the hydraulic shearing test at elevated temperature. The conductivity of the samples was measured before and after shifting the surfaces to create overriding asperities (after Stoddard et al., 2012).

5.2. Fracture Conductivity

The conductivity in the fracture and equivalent permeability were calculated using Darcy's law for linear flow.

$$Q = kA\Delta P/\mu L \quad (1)$$

where Q is the flow rate through the fracture (m3/s), k is the fracture permeability (m2), A is the cross-sectional area to flow (m2), ΔP (Pa) is the total pressure drop, μ (Pa·s) is the dynamic viscosity, and L (m) is the length over which the pressure drop is taking place. The equivalent permeability is calculated using Eq. 1 by assuming that the fluid flow axially through the entire cross section of the sample. Since it is difficult to determine the mean aperture of a fracture at different confining pressures, the conductivity is reported. Conductivity through a fracture can be calculated by multiplying the permeability by the fracture aperture,

$$D = kw_f \quad (2)$$

where D is the conductivity of the fracture, k is equivalent permeability, and W_f is the aperture of the fracture.

5.3. Experimental Results

A baseline measurement was performed at ambient temperature. Then the temperature was increased to 100°C and maintained constant for 48 hours to ensure isothermal conditions. After the system had equilibrated, the test was performed with predefined flow rates. Finally, the same procedure was repeated at a temperature of 175°C. The tests were conducted at different confining pressures. The aperture of one sample, before and after shearing, is shown in Figure 13. In Figure 14, the sample had been opened (still with the offset) and photographed. Fracture face degradation produced granite fines on the surfaces.

The experimental test conditions for flow through the split samples before and after the fracture surfaces were shifted are shown in Table 2. In order to determine the effect of surface lateral shifts on the fracture conductivity, a set of tests was run with the fracture faces shifted 2 to 2.6 mm. This was intended to simulate a fracture subjected to hydraulic shearing. From Figure 13, it is clear that the aperture of the fracture has increased significantly due to artificially realigning the surface before application of normal stress.

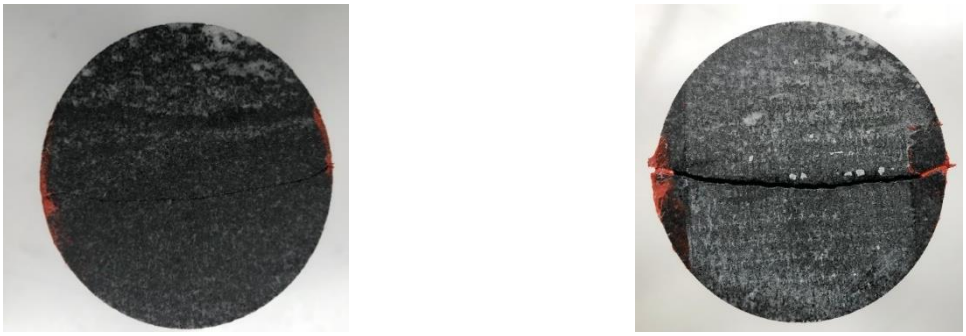

Figure 13. View of a fracture from the end of a sample (a) before shearing, (b) after shearing (simulated by manually realigning the surfaces). The orange material visible at the ends of the fracture is a flexible heat resistant membrane installed along the fracture to restrict the flow inside the fracture.

The average conductivity of the fractures before and after shearing is presented in Tables 3 and 4. The conductivity in these experiments varied by about two orders of magnitude depending on the rock properties, fracture roughness, size distribution of asperities, and mechanical properties of the fracture. The fracture conductivities of the four samples before and after the simulated shearing are presented in Figure 15. Each experiment started at room temperature and there was a relatively large variation in conductivities. With increasing time (time since load application/change is shown in the tables) and with increasing and decreasing confining pressure at various temperatures, the fractures closed and superficially equilibrated, and the degree of scatter decreased.

Figure 14. Damaged fracture surfaces after flowing under high confining pressure and temperature. The red heat-resistant epoxy was used to restrict the flow to within the fracture.

Table 3. Average conductivity of fractures before shearing.

	Conductivity (md·ft)			
Samples	**1 hr**	**48 hr**	**96 hr**	**144 hr**
1	0.851095	0.641274	0.813606	0.699195
2	1.121393	0.721777	0.492122	0.612025
3	1.891349	0.920439	0.813606	1.147381
4	9.552335	3.87476	2.729995	2.8

Table 4. The average conductivity of the fractures after shearing

Sample	Conductivity (md·ft)							
	1 hr	**48 hr**	**96 hr**	**144 hr**	**312 hr**	**480 hr**	**648 hr**	**816 hr**
1	54.68	53.39	48.44	47.65				
2	15.02	4.43	2.811	2.44				
3	292.47	151.27	87.21	58.69				
4	256.20	225.13	49.58	25.10	16.09	13.74	13.63	14.15

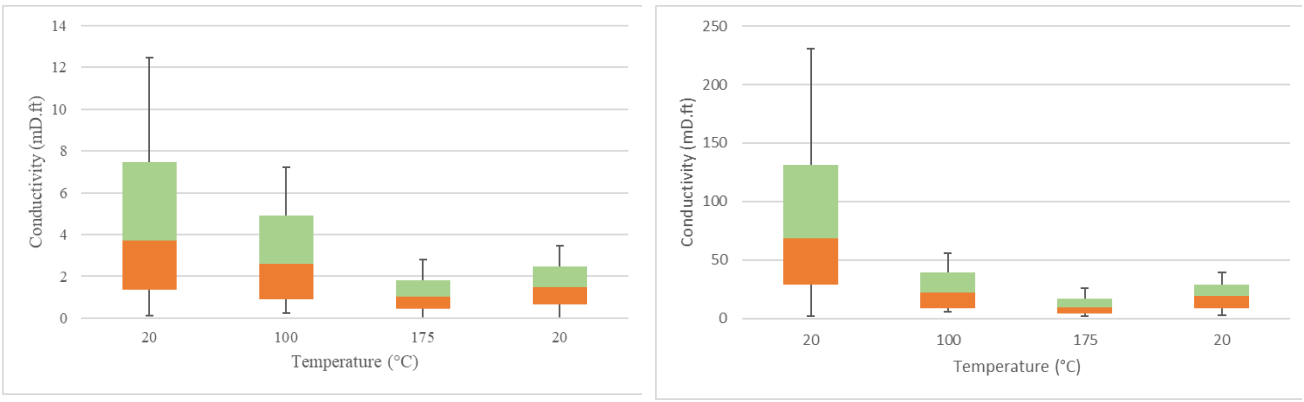

(a) Fracture conductivity before surface re-alignment. **(b) Fracture conductivity after surface re-alignment.**

Figure 15. Summary of the measured fracture conductivity of mechanically fractured granite samples (a) Fracture conductivity before shearing, (b) Fracture conductivity after shearing. Notice that the scale of the ordinate axis is different in the two panels.

5.4. Conductivity-Time Relationships

Since the average aperture of the fractures under different confining pressure was not measured, conductivity is the best metric for comparing the results. The conductivity of the fractures evaluated in the measurements significantly depends on the applied confining pressure, temperature, and time. As indicated previously, the conductivity of the fractures was measured before and after shearing under different temperature and confining pressure over a relatively representative period. Samples 1 to 3 were tested over a week (168 hours), whereas sample 4 remained at temperature and under confining pressure for 816 hours.

Figure 16 indicates that the conductivity of the fractures reduces significantly even over a one-week period. This is very evident in the case of sample 3 in which the conductivity drops to less than 30% of the value obtained at ambient temperature during the first 100 hours of loading. The conductivity of the fracture in all samples decreases significantly during the first 100 hours under elevated temperature and 2000 psi total normal stress (confining pressure). The increase in normal stress on the fracture surface due to the confining pressure and possibly thermal expansion of the rock, and broken asperities, are the main reasons for an increase in pressure difference across the samples and the associated decrease in conductivity. Granite fines – caused by broken and degraded asperities – are visible on the fracture surface each test.

The average conductivity of the fractures after shearing is shown in Table 4. Figure 17 indicates that the conductivity of the fractures in samples 3 and 4 drops significantly over the first 100 hours. As shown in Figure 17(a), the conductivity of sample 3 dropped to less than 30% of the value obtained at ambient temperature during the first 100 hours. The conductivity of sample 4 dropped to less than 20% of the value obtained at ambient temperature during the first 100 hours (see Figure 17(b)).

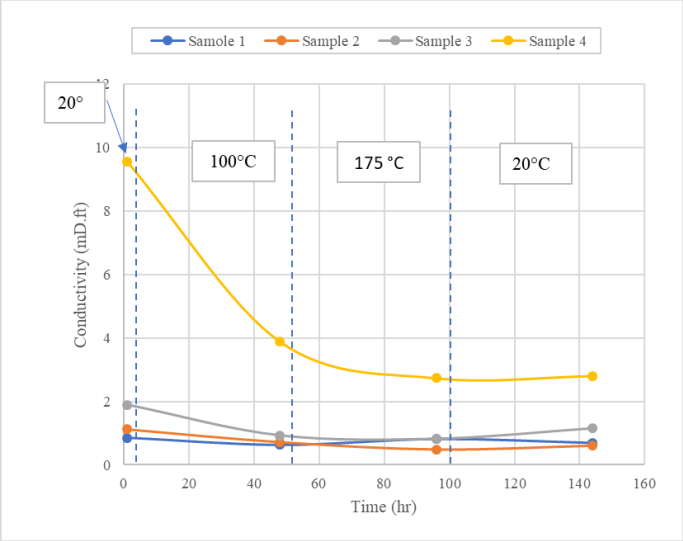

Figure 16. Average conductivity of the fractures before shearing at different temperatures.

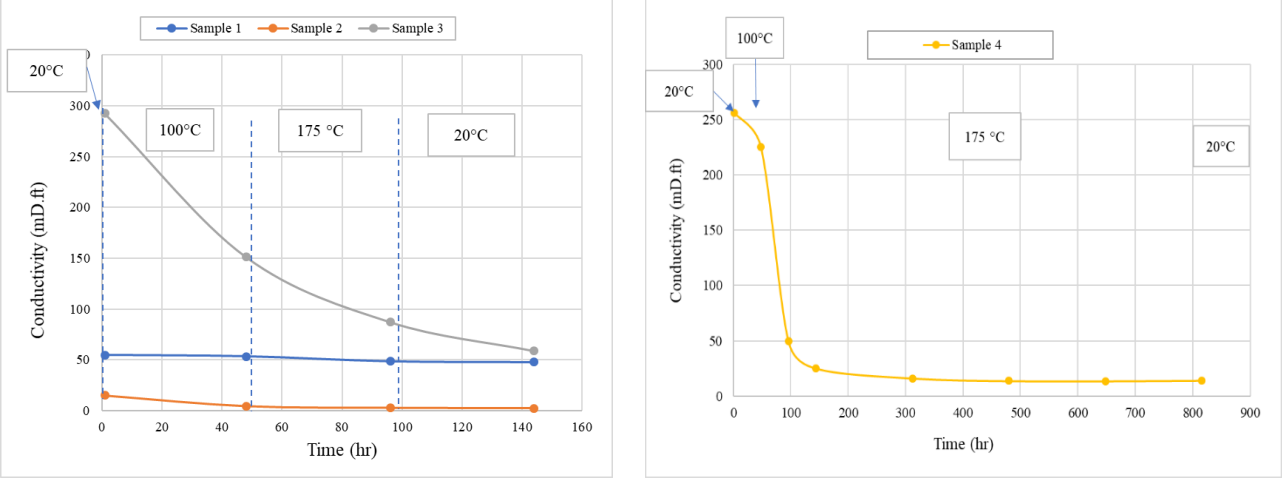

(a) **(b)**

Figure 17. Average conductivity of the fractures after simulated shearing, (a) Samples 1through 3 over a one-week period, (b) Sample 4 over 816 hours of exposure to a nominal total normal stress of 2000 psi at a temperature of 175°C.

6. CONCLUSIONS

Laboratory simulations were carried out to assess changes in fracture conductivity due to hydraulically-generated shearing and simulated shearing. Based on three types of experiments, the fracture conductivity was seen to increase significantly after shearing. Increasing the temperature and the time over which the sheared surface exists causes fracture conductivity to decrease. In the hydroshearing test, 0.09 mm of shear slip and 0.01 mm of normal dilation were induced on a saw-cut fracture in conjunction with a 2750 psi drop of the axial differential stress (zero axial strain boundary condition). As a result of this slip, the flow rate through the fracture was enhanced significantly. In another test, the flow rate/conductivity through artificially-shifted fracture surfaces increased by about two orders of magnitude, due to the large normal dilation/aperture increase caused by the artificial shear displacement. The degree of permeability enhancement depends on the rock properties, fracture roughness, size distribution of the asperities, and mechanical properties of the fracture. Finally, in a stress-dependent fluid flow test on a saw-cut fracture, increasing the confining pressure from 2000 psi to 3000 psi, resulted in a significant decrease in the flow rate. A multistage triaxial shear test on the same saw-cut fracture, indicated a fracture friction angle of 23°, with average normal and shear stiffnesses of 1.90×10^6 and 1.26×10^6 psi/in, respectively.

The laboratory experiments at temperature suggest that fracture conductivity decreases over time and this should be considered in any venture that will rely on shear stimulation alone. In some cases, the conductivity reduction was significant. For example, after only 100

hours of loading, the conductivity of one sample in particular fell to less than 30% of the conductivity at ambient temperature. The conductivity of another sample dropped to less than 20% of the value obtained at ambient temperature during the first 100 hours. The results suggest the increase in the total/effective normal stress on the fracture surface resulting from the increased confining pressure possibly combined with thermal expansion of the rock, and failed asperities, are the main reasons for the reduction in conductivity. This transient reduction in conductivity might be overcome by tensile opening associated with long-term injection of cold fluids. Regardless, it should be considered in site evaluation and conductive reservoir development.

ACKNOWLEDGMENTS

Funding for this work was provided by the U.S. DOE under grant DE-EE0007080 “Enhanced Geothermal System Concept Testing and Development at the Milford City, Utah FORGE Site”. We thank the many stakeholders who are supporting this project, including Smithfield, Utah School and Institutional Trust Lands Administration, and Beaver County as well as the Utah Governor’s Office of Energy Development.

REFERENCES

Allis, R., Gwynn, M., Hardwick, C., and Moore, J.: The challenge of correcting bottomhole temperatures–An example from FORGE 58-32, near Milford, Utah, *Stanford Geothermal Workshop* (2018).

Bauer, S. J., Huang, K., Chen, Q., and Ghassemi, A.: Laboratory and Numerical Evaluation of EGS Shear Stimulation, *Sandia National Laboratories (SNL-NM), Albuquerque, NM* (2016).

Darcy, H.: Les fontaines publiques de la ville de Dijon: exposition et application, *Victor Dalmont*, (1856).

Fredd, C. N., McConnell, S. B., and England, K. W.: Experimental study of hydraulic fracture conductivity demonstrates the benefits of using proppants, In *SPE Rocky Mountain Regional/Low-Permeability Reservoirs Symposium and Exhibition*, (2000), Society of Petroleum Engineers.

Hardwick, C. L., Gwynn, M., Allis, R., Wannamaker, P., and Moore. J.: Geophysical signatures of the Milford, Utah FORGE sit, *41st Workshop on Geothermal Reservoir Engineering*, (2016), vol. 11.

Ingebritsen, S. E., and Manning, C. E.: Permeability of the continental crust: dynamic variations inferred from seismicity and metamorphism, *Geofluids*, (2010), 10(1-2), 193-205.

Moore, D. E., Lockner, D. A., and Byerlee, J. D.: Reduction of permeability in granite at elevated temperatures, *Science*, (1994), 265 (5178):1558-1561.

Moore, J., McLennan, J., Rick, A., Kknight, P., Stuart, S., Podgorney, R., Wannamaker, P., and Wright, R.: The Utah frontier observatory for geothermal research (FORGE): results of recent drilling and geoscientific surveys, *GRC* (2018), Vol. 42.

Nadimi, S., Forbes, B., Finnila, A., Podgorney, R., Moore, J., and McLennan, J.: Hydraulic fracture/shear stimulation in an EGS reservoir: Utah FORGE program, In *52nd US Rock Mechanics/Geomechanics Symposium*, (2018), American Rock Mechanics Association.

Nemoto, K., Moriya, H., Niitsuma, H., & Tsuchiya, N. (2008). Mechanical and hydraulic coupling of injection-induced slip along pre-existing fractures. Geothermics, 37(2), 157-172, doi: 10.1016/j.geothermics.2007.11.001.

Simmons, S., Kirby, S., Jones, C., Moore, J., Allis, R., Brandt, A., and Nash, G.: The geology, geochemistry, and geohydrology of the FORGE deep well site, Milford, Utah, In *Proc. of the 43rd Workshop on Geothermal Reservoir Engineering*, (2018).

Stoddard, T., McLennan, J, and Moore, J.: Fracture conductivity of a bauxite-propped geothermal system at in-situ conditions, In *Thirty-Sixth Workshop on Geothermal Reservoir Engineering, Stanford University, Stanford* (2012).

Whitaker, S.: Flow in porous media I: A theoretical derivation of Darcy's law, *Transport in Porous Media* (1986), 1 (1):3-25.

Yasuhara, H., Polak, A., Mitani, Y., Grader, A. S., Halleck, P. H., and Elsworth, D.: Evolution of fracture permeability through fluid–rock reaction under hydrothermal conditions, *Earth and Planetary Science Letters*, (2006), 244 (1-2):186-200.

Ye, Z., and Ghassemi, A.: Deformation Properties of Saw-Cut Fractures in Barnett, Mancos and Pierre Shales, *Proceedings*, 50th US Rock Mechanics/Geomechanics Symposium, Houston, TX (2016).

Ye, Z., Janis, M., & Ghassemi, A.: Injection-driven Shear Slip and The Coupled Permeability Evolution of Granite Fractures for EGS Stimulation, In *51st US Rock Mechanics/Geomechanics Symposium*, (2017), American Rock Mechanics Association.

Ye, Z., and Ghassemi, A.: Injection-Induced Shear Slip and Permeability Enhancement in Granite Fractures. Journal of Geophysical Research, *Solid Earth*, (2018), 123(10), 9009-9032.